Journal of Computational Physics 283 (2015) 23–36

Contents lists available at ScienceDirect

Journal of Computational Physics

www.elsevier.com/locate/jcp

Removal of pseudo-convergence in coplanar and near-coplanar Riemann problems of ideal magnetohydrodynamics solved using finite volume schemes

A.D. Kercher *, R.S. Weigel

School of Physics, Astronomy, and Computational Sciences, George Mason University, Fairfax, VA, United States

ARTICLE INFO

Article history:
Received 5 June 2014
Received in revised form 12 November 2014
Accepted 21 November 2014
Available online 29 November 2014

Keywords:
Finite volume
Ideal MHD
Coplanar
Pseudo-convergence

ABSTRACT

Numerical schemes for ideal magnetohydrodynamics (MHD) that are based on the standard finite volume method (FVM) exhibit pseudo-convergence in which irregular structures no longer exist only after heavy grid refinement. We describe a method for obtaining solutions for coplanar and near-coplanar cases that consist of only regular structures, independent of grid refinement. The method, referred to as Compound Wave Modification (CWM), involves removing the flux associated with non-regular structures and can be used for simulations in two- and three-dimensions because it does not require explicitly tracking an Alfvén wave. For a near-coplanar case, and for grids with 2^{13} points or less, we find root-square-mean-errors (RMSEs) that are as much as 6 times smaller. For the coplanar case, in which non-regular structures will exist at all levels of grid refinement for standard FVMs, the RMSE is as much as 25 times smaller.

1. Introduction

A Riemann problem is a one-dimensional initial value problem for a conservative system in which a single discontinuity separates two constant states. Riemann problems play an important role in fluid simulations; numerical algorithms in both computational fluid dynamics (CFD) and computational MHD use linear approximations of local Riemann problems for the computation of numerical fluxes [3,6,19].

The ideal MHD equations are more complex than the Euler equations of hydrodynamics. As a result, the number of possible structures is greater for ideal MHD. In addition, the system of equations is non-strictly hyperbolic, which makes non-regular structures such as intermediate shocks and compound waves possible.

Solutions of Riemann problems are composed of multiple structures that emanate away from a discontinuity. A solution is only considered physical if it satisfies entropy and evolutionary conditions [14]. The entropy is $S = p_g/\rho^\gamma$, where p_g is the gas pressure, ρ is the density, and γ is the ratio of specific heats. The entropy condition states that the change in entropy across a shock is zero or larger. The evolutionary condition requires a shock to be structurally stable under small perturbations [14]. In hydrodynamics, the entropy and evolutionary conditions are equivalent.

In the past, intermediate shocks in ideal MHD have been considered unphysical because they are structurally unstable under small perturbations [15]. In recent years, their physicality has been reconsidered. Observations of heliospheric plasma and numerical simulations of bow shocks have provided evidence for their existence. Feng and Wang [11] reported that a

* Corresponding author. Tel.: +1 703 993 1361; fax: +1 703 993 1269.
E-mail addresses: akercher@gmu.edu (A.D. Kercher), rweigel@gmu.edu (R.S. Weigel).

http://dx.doi.org/10.1016/j.jcp.2014.11.027
0021-9991/

discontinuity observed by *Voyager* 2 in January 1979 was an intermediate shock. Chao et al. [4] identified an intermediate shock in *Voyager* 1 measurements in 1980. Intermediate shocks have been observed in numerical simulations of bow shocks in both two- and three-dimensions [7,8]. They were first observed in numerical simulations by Brio and Wu [3] whose results have been used extensively as a reference for numerical solutions of the ideal MHD equations. An exact nonlinear solver for ideal MHD that accounts for intermediate shocks was developed by Takahashi and Yamada [22] to investigate non-unique solutions to Riemann problems of ideal MHD. They showed that there were uncountably many non-regular solutions, but only one regular solution to the Riemann problem described by Brio and Wu.

The convergence rates for various implementations of the finite volume method on one-dimensional Riemann problems with non-unique solutions were computed by Torrilhon [24]. All implementations exhibited non-uniform convergence with respect to grid resolution. The schemes produced solutions that converged toward the non-regular solution until a certain level of grid refinement, at which point convergence was to the regular solution. This behavior was referred to as pseudo-convergence, and numerical diffusion was identified as the cause. For the coplanar case, in which the rotation angle is 180°, we argue that convergence to the non-regular solution is expected to always occur, independent of grid resolution, because the transverse velocity and magnetic field are restricted to a single plane.

Because grids with more than 10^4 points are needed to obtain L^1 errors on the order of 10^{-2}, Torrilhon [24] suggested using adaptive mesh refinement (AMR) to reduce the computational costs. AMR can be a powerful computational tool but is complex to implement, and for structured grids, it introduces non-conformity. High order weighted essentially non-oscillatory (WENO) schemes were investigated by Torrilhon and Balsara [26]. The schemes have a spatial accuracy of $2r-1$ in regions where the solution is smooth. They reported results using $r=3$ and $r=5$, giving fifth and ninth order accuracy in space respectively. The higher order schemes converged to the regular solution on coarser grids and were able to obtain L^1 errors on the order of 10^{-2} with half the grid resolution that lower order schemes require, but they still exhibited pseudo-convergence.

We introduce an alternative method for error reduction that does not exhibit pseudo-convergence, Compound Wave Modification (CWM), that requires modifying the flux from the finite volume approximation. The modification is done to the Harden–Lax–van Leer-Discontinuities (HLLD) [18] approximate Riemann solver implemented in the *Athena* MHD code [21,20]. The CWM solutions are compared with one-dimensional exact solutions for a near-coplanar case and the coplanar case. The exact solutions are found using a non-linear Riemann solver that is based on the method described by Dai and Woodward [6] with the rarefaction wave extension by Ryu and Jones [19].

CWM is only suitable for problems of ideal MHD since it is designed to converge to the solution containing regular waves. Evidence suggests non-regular waves are physically admissible for dissipative, non-ideal MHD. Intermediate shocks have been shown to form by wave steepening in the case of dissipative MHD [27,29]. Wu later argued that rotational discontinuities are unstable and will evolve into intermediate shocks in the case of dissipative MHD [28,30]. Time dependent intermediate shocks (TDIS), which do not satisfy the Rankine–Hugoniot, connect two near coplanar states and were also observed in dissipative MHD [31]. Torrilhon [24] compared the behavior of TDIS with pseudo-convergence, in which the regular solution is only obtained after long times in the case of TDIS and for fine grids in the case of pseudo-convergence. Inoue and Inutsuka [12] expanded on earlier finding on the physical admissibility of intermediate shocks in non-ideal MHD to the case of resistive MHD without viscosity. Intermediate shocks may be a physical solution for dissipative MHD therefore the use of CWM would not be appropriate.

The remainder of this paper is organized as follows. In Section 2.1, the MHD equations are presented. In Section 2.2, the classification of the possible discontinuities and shocks of ideal MHD are described. In Section 2.3, an overview of the numerical methods implemented in Riemann solvers is given. In Section 3, Riemann problems with non-unique solutions are introduced and the test cases are described. In Section 4, the CWM method is described and convergence to the correct solution is demonstrated.

2. Ideal MHD and numerical methods

2.1. Ideal MHD

The ideal MHD equations are an approximate description of the interaction between plasma flowing in a region with a magnetic field. They consist of the Euler equations of hydrodynamics and the magnetic induction equation, $\frac{\partial \mathbf{B}}{\partial t} = \nabla \times (\mathbf{v} \times \mathbf{B}) + \eta \nabla^2 \mathbf{B}$, for which the divergence-free condition $\nabla \cdot \mathbf{B} = 0$ is satisfied. The effects of resistivity, thermal conductivity, and viscosity are neglected. The equations are

$$\frac{\partial \rho}{\partial t} + \nabla \cdot (\rho \mathbf{v}) = 0, \tag{2.1}$$

$$\frac{\partial (\rho \mathbf{v})}{\partial t} + \nabla \cdot \left[\rho \mathbf{v} \otimes \mathbf{v} + \left(p_g + \frac{B^2}{2} \right) \underline{\mathbf{I}} - \mathbf{B} \otimes \mathbf{B} \right] = 0, \tag{2.2}$$

$$\frac{\partial E}{\partial t} + \nabla \cdot \left[\left(E + p_g + \frac{B^2}{2} \right) \mathbf{v} - \mathbf{v} \cdot \mathbf{B} \otimes \mathbf{B} \right] = 0, \quad \text{and} \tag{2.3}$$

$$\frac{\partial \mathbf{B}}{\partial t} + \nabla \cdot [\mathbf{v} \otimes \mathbf{B} - \mathbf{B} \otimes \mathbf{v}] = 0, \tag{2.4}$$

where the energy density is defined as

$$E = \frac{p_g}{\gamma - 1} + \frac{\rho v^2}{2} + \frac{B^2}{2}, \tag{2.5}$$

the gas constant γ is the ratio of specific heats, and B is the magnitude of the magnetic field. The units are chosen so that the speed of light c and constant 4π do not appear in the equations.

In one dimension, with flow variation in the x-direction, the ideal MHD equations can be written in the form of a conservation law

$$\frac{\partial \mathbf{U}}{\partial t} + \frac{\partial \mathbf{F}}{\partial x} = \mathbf{0},$$

where the conservative state variables $\mathbf{U}$ and their respective fluxes $\mathbf{F}$ are

$$\mathbf{U} = \begin{bmatrix} \rho \\ \rho v_n \\ \rho \mathbf{v}_t \\ E \\ \mathbf{B}_t \end{bmatrix}, \qquad \mathbf{F} = \begin{bmatrix} \rho v_n \\ \rho v_n^2 + p_g + B^2/2 - B_n^2 \\ \rho v_n \mathbf{v}_t - B_n \mathbf{B}_t \\ (E + p_g + B^2/2) v_n - (\mathbf{v} \cdot \mathbf{B}) B_n \\ v_n \mathbf{B}_t - B_n \mathbf{v}_t \end{bmatrix},$$

and a normal (x) component is denoted with the subscript n and tangential components are denoted with the subscript t. The normal component of the magnetic field is treated as a parameter because it must be constant in order to satisfy the divergence-free condition of $\mathbf{B}$, which is $\partial B_n / \partial x = 0$ in one dimension.

The Jacobian matrix, $\mathbf{J}(\mathbf{U}) = \partial \mathbf{F} / \partial \mathbf{U}$, has real but not necessarily distinct eigenvalues in ideal MHD. The ideal MHD system is called non-strictly hyperbolic because it can have degenerate eigenvalues. Each eigenvalue is associated with a wave that travels at the characteristic speed

v_n: contact or tangential discontinuity (entropy),

$v_n \pm c_s$: slow rarefaction or shock,

$v_n \pm c_a$: rotational discontinuity (Alfvén), and

$v_n \pm c_f$: fast rarefaction or shock,

where c_s, c_a, c_f are the slow, Alfvén, and fast wave propagation speeds, respectively. The sign in each equation indicates the direction of propagation. The propagation speeds are

$$c_{f,s}^2 = \frac{1}{2}\left[a^2 + c_a^2 + c_t^2 \pm \sqrt{\left(a^2 + c_a^2 + c_t^2\right)^2 - 4a^2 c_a^2}\right] \quad \text{and} \quad c_a^2 = \frac{B_n^2}{\rho},$$

where $c_t^2 = B_t^2/\rho$, $a^2 = \gamma p_g / \rho$, c_a (c_t) is the Alfvén speed normal (tangential) to the wave front, and a is the speed of sound. The plus (minus) sign corresponds to the fast (slow) propagation speed.

2.2. Discontinuities and shock classification

In ideal MHD, a contact discontinuity (CD) has a discontinuous jump in density that occurs where the normal component of the magnetic field is nonzero and the velocity, gas pressure, and tangential components of the magnetic field are continuous. The heliopause and magnetopause are two astrophysical boundaries where plasma flows are separated by a density discontinuity. If the normal component of the magnetic field is zero, the contact discontinuity is referred to as a tangential discontinuity. For a tangential discontinuity, only the normal velocity and total pressure (gas plus magnetic pressure) are continuous [13].

Shocks are typed by comparing the pre-shock and post-shock velocities with the characteristic velocities in the respective states. Numbers are assigned to the state according to the inequalities $4 < c_s < 3 < c_a < 2 < c_f < 1$. If $|v_n| > c_f$, a state is referred to as superfast and denoted 1; if $|v_n| = c_f$, it is referred to as fast and denoted $1, 2$; if $|v_n| < c_f$ it is referred to as subfast and denoted 2. When $|v_n| = c_a$, it is referred to as an Alfvén shock and denoted $2, 3$. The shock is referred to as superslow (3) if $|v_n| > c_s$, slow $(3, 4)$ if $|v_n| = c_s$, and subslow (4) if $|v_n| < c_s$. Finally, the shock is classified as static if $|v_n| = 0$. Shocks are then classified as an $i \to j$ type where i is the upstream type and j is the downstream type.

- $1 \to 2$ fast shocks (FSs) have compression and increase in strength of the tangential magnetic field as the shock front is transversed: $B_{t1} < B_{t2}$.
- $3 \to 4$ slow shocks (SSs) have compression and a decrease in strength of the tangential magnetic field as the shock front is transversed: $B_{t1} > B_{t2}$.
- $1 \to 2, 3$ (switch-on) shocks have a tangential magnetic field that is zero upstream and nonzero downstream: $B_{t1} = 0$ and $B_{t2} \neq 0$.

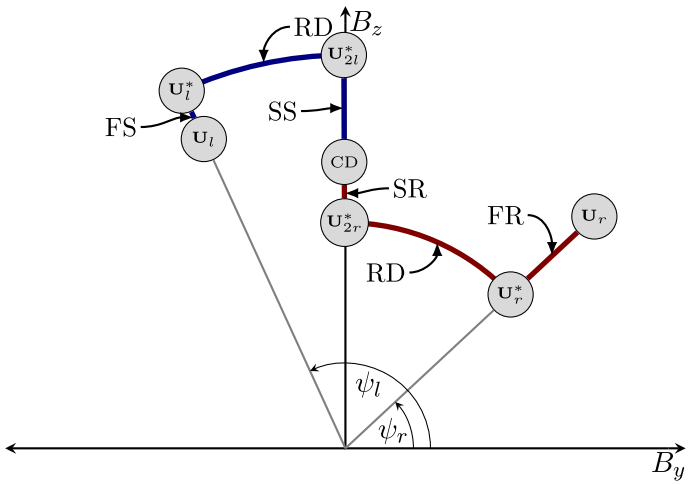

Fig. 1. The influence of regular structures on the tangential magnetic field. The orientation angle is $\psi = \tan B_z/B_y$. Regular structures only influence the magnitude or orientation of the perpendicular magnetic field. The intermediate states, $\mathbf{U}^*$, are defined in Fig. 2.

- $2, 3 \to 4$ (switch-off) shocks have a tangential magnetic field that is nonzero upstream and zero downstream: $B_{t1} \neq 0$ and $B_{t2} = 0$.
- $1 \to 3$, $1 \to 4$, $2 \to 3$ and $2 \to 4$ intermediate shocks (ISs) have a change in sign of the tangential magnetic field as the shock front is transversed: $B_{t1} < 0 < B_{t2}$ or $B_{t1} > 0 > B_{t2}$.

So-called regular waves only influence the orientation of the perpendicular magnetic field or its magnitude. Fast and slow shocks alter the magnitude of the perpendicular magnetic field while rotational discontinuities alter their orientation (see Fig. 1). A rotational discontinuity (RD) propagates with a speed of c_a and rotates the perpendicular magnetic field while the magnitude of the perpendicular magnetic field is equal on both sides of the discontinuity. Expansion waves can also occur in ideal MHD. The magnitude of the tangential magnetic field will decrease across fast rarefactions (FRs); across slow rarefactions (SRs) it will increase.

Intermediate shocks are over-compressive shocks that alter both the magnitude and orientation of the tangential magnetic field. These shocks are classified as $1 \to 3$, $1 \to 4$, $2 \to 4$, and $2 \to 3$. The $2 \to 3$ class is called an Alfvén shock and across it the tangential magnetic field rotates by 180°. A switch-on shock ($1 \to 2, 3$) corresponds to a pre-shock tangential magnetic field of zero and a non-zero post shock tangential magnetic field. A switch-off shock ($2, 3 \to 4$) occurs when the tangential magnetic field is zero post-shock.

2.3. Numerical methods

2.3.1. Nonlinear Riemann solver

Analytic solutions to problems of ideal MHD are generally not known. However, highly accurate, to machine precision, solutions can be generated using a nonlinear solver [6,19,23]. The exact solutions presented in this work were found using a nonlinear solver that is based on the method originally developed by Dai and Woodward [6] and improved by Ryu and Jones [19] to correctly compute rarefaction waves.

The exact solutions are composed of eight possible MHD states separated by seven wave fronts, as depicted in Fig. 2. The transitions from one region to another through a discontinuity is controlled by the jump conditions associated with the discontinuity. The Rankine–Hugoniot jump conditions for ideal MHD in Lagrangian mass coordinates, $dm = \rho dx$, are

$$W[V] = -[v_n], \tag{2.6}$$

$$W[v_n] = -\left[P - B_n^2\right], \tag{2.7}$$

$$W[\mathbf{v}_t] = -B_n[\mathbf{B}_t], \tag{2.8}$$

$$W[V\mathbf{B}_t] = -B_n[\mathbf{v}_t], \quad \text{and} \tag{2.9}$$

$$W[VE] = [v_n P] - B_n[B_n v_n + \mathbf{B}_t \cdot \mathbf{v}_t], \tag{2.10}$$

where $P = p_g + \frac{1}{2}(B_n^2 + B_t^2)$ is the total pressure and $W = -(\rho v_n)_u = -(\rho v_n)_d$ is the Lagrangian velocity of the discontinuity and $V = 1/\rho$ [6,19]. When moving in the $-x$ direction, the velocity W is negative. Brackets are used to denote the difference between the upstream and downstream states for a quantity Q, i.e. $[Q] = Q_u - Q_d$.

Dai and Woodward [6] give the fast and slow shock speeds in mass coordinates as

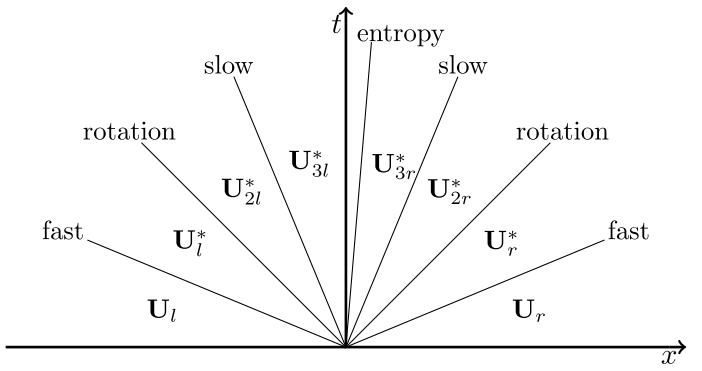

Fig. 2. Seven possible waves and/or discontinuities separating the eight possible states of the ideal MHD Riemann problem. The initial contact discontinuity, i.e., the entropy wave, separates states $\mathbf{U}^*_{3l}$ and $\mathbf{U}^*_{3r}$.

$$W^2_{f,s} = \frac{1}{2(1+S_0)}\left[\left(C_s^2 + C_f^2 + S_1^2\right) \pm \sqrt{\left(C_s^2 + C_f^2 + S_1^2\right)^2 - 4(1+S_0)\left(C_s^2 C_f^2 - S_2\right)}\right], \tag{2.11}$$

where $C_f = \rho c_f$ and $C_s = \rho c_s$. The quantities S_0, S_1, S_2 are given by Ryu and Jones [19] in terms of B_t as

$$S_0 = -\frac{1}{2}(\gamma - 1)\frac{[B_t]}{B_t}, \tag{2.12}$$

$$S_1 = \frac{1}{2}\left\{-(\gamma-2)VC_t^2\frac{[B_t]}{B_t} + 2C_0^2 - (\gamma-4)VC_t^2 - 2\gamma C_a^2\right\}\frac{[B_t]}{B_t}, \quad \text{and} \tag{2.13}$$

$$S_2 = \frac{1}{2}\left\{\frac{C_a^2[B_t]^2}{V} + (\gamma+2)C_tC_a^2[B_t] + VC_t^2C_a^2(\gamma+1) + (\gamma+1)C_a^4 - 2C_0^2C_a^2\right\}\frac{[B_t]}{B_t}, \tag{2.14}$$

where $C_0 = \rho a$ is the Lagrangian speed of sound, $C_a = \rho c_a$ is the Lagrangian Alfvén speed, and $C_t = \sqrt{\rho B_t^2}$. The quantities in Eqs. (2.12)–(2.14) are for the state downstream of the shock.

The relationships for fast rarefactions given by Ryu and Jones [19] are

$$\frac{dC_0}{dB_t} = -\frac{\gamma+1}{2}\sqrt{\rho}\frac{C_tC_s^2}{C_0(C_s^2 - C_a^2)} = \frac{\gamma+1}{2}\sqrt{\rho}\frac{C_s^2(C_f^2 - C_a^2)}{C_a^2C_tC_0} = \frac{\gamma+1}{2}\frac{\rho}{C_0}\frac{dp_g}{dB_t}, \tag{2.15}$$

$$\frac{dv_n}{dB_t} = \mp\frac{1}{\sqrt{\rho}}\frac{C_\perp C_a^2}{C_f(C_s^2 - C_a^2)} = \pm\frac{C_f^2 - C_a^2}{\sqrt{\rho}C_tC_f} = \pm\frac{2}{\gamma+1}\frac{C_0C_a^2}{C_s^2C_f}\frac{1}{\rho}\frac{dC_0}{dB_t}, \quad \text{and} \tag{2.16}$$

$$\frac{1}{\cos\psi}\frac{dv_{t1}}{dB_t} = \frac{1}{\sin\psi}\frac{dv_{t2}}{dB_t} = \mp\frac{1}{\sqrt{\rho}}\frac{C_a}{C_f}, \tag{2.17}$$

where the upper and lower signs refer to right- and left-going waves, respectively. The rotation angle is defined by $\tan\psi = B_z/B_y$.

For slow rarefactions, replace the fast speed (C_f) with the slow speed (C_s) and the slow speed (C_s) with the fast speed (C_f) in Eqs. (2.15)–(2.17).

An initial guess for the solution in the six interior regions shown in Fig. 2 is improved iteratively until the jump conditions of the initial contact or tangential discontinuity are satisfied to within a desired accuracy. We have found a very high rate of convergence using the intermediate states approximated using the HLLD method for the initial guess. In practice, we use a relaxation factor and apply damping to speed up convergence.

2.3.2. Approximate Riemann solver

Approximate solutions were obtained with version 4.2 of Athena. All approximate solutions were computed with the corner-transport-upwind (CTU) method. Spatial reconstruction of the interface states was done using the third-order-accurate piecewise-parabolic method (PPM) of Colella and Woodward [5]. The fluxes were approximated with the HLLD method developed by Miyoshi and Kusano [18]. We have included a brief description below.

An MHD extension of the HLL scheme [9] capable of resolving all isolated linear discontinuities of ideal MHD, i.e. RDs and CDs, was developed by Miyoshi and Kusano [18]. They referred to the scheme as HLLD, where the D stands for *discontinuities*. The HLLD scheme assumes a six-state solution separated by five waves as depicted in Fig. 3. Two nonlinear waves, i.e., shocks and rarefactions, separate the left and right initial states from the intermediate states in the Riemann fan, i.e., $\mathbf{U}^*_l$, $\mathbf{U}^*_{2l}$, $\mathbf{U}^*_{2r}$, and $\mathbf{U}^*_r$. The four intermediate states are separated by two RDs with velocities, S^*_l, S^*_r, and one CD with velocity, S_m. Details for approximating the waves speeds and intermediate states are given in [18].

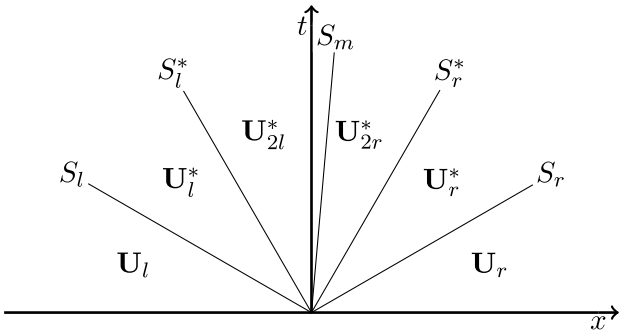

Fig. 3. Intermediate states and waves used in the HLLD approximate Riemann solver.

The HLLD fluxes are found by applying the integral conservation laws over the left half or right half of the Riemann fan, $(S_l\delta t, 0)\times(0,\delta t)$ or $(0, S_r\delta t)\times(0,\delta t)$, see [18]. The fluxes (e.g., Eq. (66) of [18]) are

$$\mathbf{F}(x,t) = \begin{cases} \mathbf{F}_l & \text{if } 0 < S_l, \\ \mathbf{F}_l^* = \mathbf{F}_l + S_l(\mathbf{U}_l^* - \mathbf{U}_l) & \text{if } S_l \le 0 \le S_l^*, \\ \mathbf{F}_{2l}^* = \mathbf{F}_l^* + S_l^*(\mathbf{U}_{2l}^* - \mathbf{U}_l^*) & \text{if } S_l^* \le 0 \le S_m, \\ \mathbf{F}_{2r}^* = \mathbf{F}_r^* + S_r^*(\mathbf{U}_{2r}^* - \mathbf{U}_r^*) & \text{if } S_m \le 0 \le S_r^*, \\ \mathbf{F}_r^* = \mathbf{F}_r + S_r(\mathbf{U}_r^* - \mathbf{U}_r) & \text{if } S_r^* \le 0 \le S_r, \\ \mathbf{F}_r & \text{if } S_r < 0. \end{cases} \tag{2.18}$$

The HLLD method serves as the base approximate Riemann solver in this paper. The intermediate states approximated during the HLLD flux computation will be used as the initial conditions of the reduced Riemann problem in CWM described in Section 4. This provides a drastic performance increase over use of an exact Riemann solver.

3. Riemann problems with non-unique solutions

Unique solutions to Riemann problems of ideal MHD are not guaranteed. For certain initial conditions, the Riemann problem will have non-unique solutions. Non-unique solutions will occur for problems with coplanar (anti-parallel) magnetic fields [1]. One solution has a 180° rotational discontinuity and slow shock and the other solution has a compound wave. A method for constructing Riemann problems with non-unique solutions and non-planar initial conditions is given by Torrilhon [25]. As with the coplanar case, one solution consists of a 180° rotational discontinuity and a slow shock and the other solution has a compound wave. As discussed in this section, for cases with a 180° rotation in the solution (either a compound wave or rotational discontinuity), convergence to the solution containing only a rotational discontinuity is impossible with numerical approximations based on the finite volume method.

Using the same terminology and notation as Torrilhon [24], intermediate shocks and compound waves are referred to as non-regular structures. Regular structures include rarefactions, linear discontinuities, and Lax shocks. The solution of the ideal MHD Riemann problem that includes only regular structures is referred to as the r-solution. The solution that contains a compound wave is referred to as the c-solution.

In this work, we consider the coplanar and near coplanar Riemann problems of two test cases. The first case was described by Torrilhon [24]. The initial conditions and parameters used here are equivalent but have been scaled to the unit interval $[0,1]$ using

$$\hat{\rho} = \frac{\rho}{\rho_l}, \qquad \hat{\mathbf{v}} = \frac{\mathbf{v}}{a_l}, \qquad \hat{\mathbf{B}} = \frac{\mathbf{B}}{\sqrt{\gamma\, p_{gl}}}, \qquad \hat{p}_g = \frac{p_g}{\gamma\, p_{gl}}, \qquad \hat{L}_x = 1, \quad \text{and} \quad \hat{t}_f = \frac{a_l t_f}{L_x}.$$

The initial conditions are

$$\begin{aligned} (\rho_l, v_{nl}, \mathbf{v}_{tl}, p_{gl}, \mathbf{B}_{tl}) &= \big(1.0.0, 0.0, (0.0, 0.0), 0.5, (0.7746, 0.0)\big), \\ (\rho_r, v_{nr}, \mathbf{v}_{tr}, p_{gr}, \mathbf{B}_{tr}) &= \big(0.2, 0.0, (0.0, 0.0), 0.12, 0.7746(\cos\alpha, \sin\alpha)\big), \end{aligned} \tag{3.1}$$

where $B_n = 0.7746$, and $\gamma = 5/3$, and $\alpha = 3.0, \pi$. The initial discontinuity is located at $x = 0.4$ for comparison with the results in [24]. The exact solution for $\alpha = \pi$ (3.0) is listed in Tables 1, 2. The exact and approximate solutions of the coplanar case are shown in Fig. 4 at time $t_f = 0.20656$.

Test 2 is similar to Test 5b of [19]. The initial conditions are

$$\begin{aligned} (\rho_l, v_{nl}, \mathbf{v}_{tl}, p_{gl}, \mathbf{B}_{tl}) &= \big(1.0.0, 0.0, (0.0, 0.0), 0.5, (1.0, 0.0)\big), \\ (\rho_r, v_{nr}, \mathbf{v}_{tr}, p_{gr}, \mathbf{B}_{tr}) &= \big(0.2, 0.0, (0.0, 0.0), 0.12, (\cos\alpha, \sin\alpha)\big), \end{aligned} \tag{3.2}$$

Table 1
Exact solution of Test 1 (3.1) with $\alpha = \pi$.

ρ	v_n	v_y	v_z	p_g	B_t	ψ
1.0000E+0	0.0000E+0	0.0000E+0	0.0000E+0	6.0000E−1	7.7460E−1	0.0000E+0
6.9269E−1	4.6523E−1	−2.8989E−1	0.0000E+0	3.2580E−1	3.8383E−1	0.0000E+0
6.9269E−1	4.6523E−1	−1.2122E+0	0.0000E+0	3.2580E−1	3.8383E−1	3.1416E+0
7.6860E−1	3.9016E−1	−1.1190E+0	0.0000E+0	3.8764E−1	3.2045E−1	3.1416E+0
3.6449E−1	3.9016E−1	−1.1190E+0	0.0000E+0	3.8764E−1	3.2045E−1	3.1416E+0
1.7257E−1	−3.6407E−1	−3.5772E−1	0.0000E+0	9.3845E−2	5.6339E−1	3.1416E+0
1.7257E−1	−3.6407E−1	−3.5772E−1	0.0000E+0	9.3845E−2	5.6339E−1	3.1416E+0
2.0000E−1	0.0000E+0	0.0000E+0	0.0000E+0	1.2000E−1	7.7460E−1	3.1416E+0

$B_n = 0.7746$.

Table 2
Exact solution of MHD Test 1 (3.1) with $\alpha = 3.0$.

ρ	v_n	v_y	v_z	p_g	B_t	ψ
1.0000E+0	0.0000E+0	0.0000E+0	0.0000E+0	6.0000E−1	7.7460E−1	0.0000E+0
6.9410E−1	4.6286E−1	−2.8778E−1	0.0000E+0	3.2690E−1	3.8603E−1	0.0000E+0
6.9410E−1	4.6286E−1	−1.2000E+0	1.1481E−1	3.2690E−1	3.8603E−1	2.8912E+0
7.6755E−1	3.9041E−1	−1.1126E+0	9.2456E−2	3.8673E−1	3.2483E−1	2.8912E+0
3.6442E−1	3.9041E−1	−1.1126E+0	9.2456E−2	3.8673E−1	3.2483E−1	2.8912E+0
1.7295E−1	−3.5886E−1	−3.7704E−1	−9.5671E−2	9.4188E−2	5.6658E−1	2.8912E+0
1.7295E−1	−3.5886E−1	−3.4819E−1	4.9634E−2	9.4188E−2	5.6658E−1	3.0000E+0
2.0000E−1	0.0000E+0	0.0000E+0	0.0000E+0	1.2000E−1	7.7460E−1	3.0000E+0

$B_n = 0.7746$.

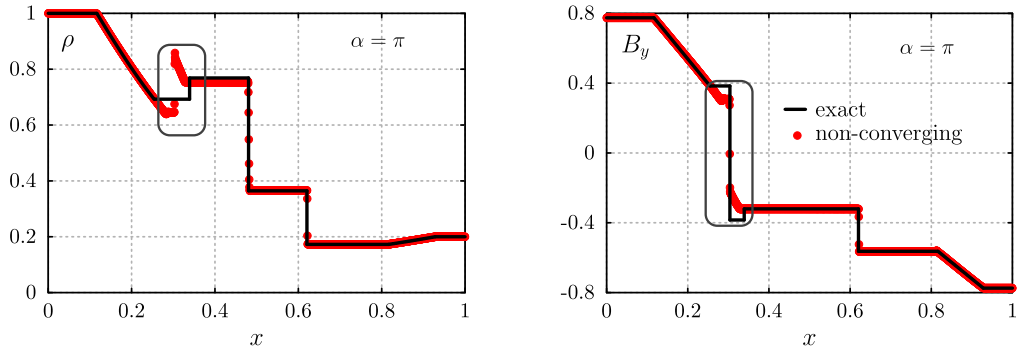

Fig. 4. Non-convergence for the coplanar case of Test 1. An irregular structure (slow compound wave) in the approximate solution exists in place of the rotational discontinuity in the exact solution at $x = 0.303$. The domain used for error analysis is $x = [0.254, 0.481]$.

where $B_n = 1.25$, $\gamma = 5/3$, and $\alpha = 3.0, \pi$. The initial discontinuity is located at $x = 0.5$. The exact solution for $\alpha = \pi$ (3.0) is listed in Tables 3, 4. The exact and approximate solutions of the coplanar case are shown in Fig. 5 at time $t_f = 0.15$.

The exact solution containing only regular structures and the approximate solution containing a compound wave are shown in Fig. 4. For a numerical scheme to converge to the r-solution, the density and the magnitude of the transverse magnetic field must remain constant between the left-going fast and slow structures, shown in Fig. 4 at $x = 0.254$ and $x = 0.339$ respectively, otherwise a compound wave will appear.

Falle and Komissarov [10] described the appearance of compound waves in numerical simulations in terms of the properties of the planar ideal MHD equations. In this case, the system of equations is reduced from seven to five by removing the equations for the z-component of the velocity and magnetic field. In the reduced system, the Alfvén waves are lost but the other characteristic fields are unchanged. The Alfvén velocity is no longer a characteristic speed of the system but rotational discontinuities still satisfy the jump conditions and propagate at that velocity. In planar ideal MHD, a rotational discontinuity can only rotate the perpendicular magnetic field by 180° because it is restricted to a single plane.

Finite volume methods have no way of compensating for the reduction in dimension in the planar case. If one of the perpendicular components of velocity and magnetic field vanish, there is no mechanism to transfer energy between the perpendicular field components across the rotational discontinuity. The field in a cell would need to undergo a full 180° rotation in one time step in order for the magnitude of the perpendicular magnetic field to remain constant. Numerical diffusion and stability constraints prohibit the full rotation from being realized in one time step. In addition, any interpolation with order greater than piecewise constant will produce a magnetic field at the cell interface (where the flux is calculated) with a magnitude that is less than that in the center of the adjoining cells. From Eq. (2.5), any change in kinetic or magnetic energy will result in an increase in gas pressure that is connected to the upstream state through a shock and

Table 3
Exact solution of Test 2 (3.2) with $\alpha = \pi$.

ρ	v_n	v_y	v_z	p_g	B_t	ψ
1.0000E+0	0.0000E+0	0.0000E+0	0.0000E+0	1.0000E+0	1.0000E+0	0.0000E+0
7.1386E−1	5.8342E−1	−5.6703E−1	0.0000E+0	5.6951E−1	3.5206E−1	0.0000E+0
7.1386E−1	5.8342E−1	−1.4004E+0	0.0000E+0	5.6951E−1	3.5206E−1	3.1416E+0
8.8546E−1	3.4177E−1	−1.2411E+0	0.0000E+0	8.1810E−1	2.3864E−1	3.1416E+0
6.4157E−1	3.4177E−1	−1.2411E+0	0.0000E+0	8.1810E−1	2.3864E−1	3.1416E+0
3.2226E−1	−5.4352E−1	−7.5467E−1	0.0000E+0	2.3251E−1	4.6173E−1	3.1416E+0
3.2226E−1	−5.4352E−1	−7.5467E−1	0.0000E+0	2.3251E−1	4.6173E−1	3.1416E+0
4.0000E−1	0.0000E+0	0.0000E+0	0.0000E+0	3.3333E−1	1.0000E+0	3.1416E+0

$B_n = 1.25$.

Table 4
Exact solution of MHD Test 2 (3.2) with $\alpha = 3.0$.

ρ	v_n	v_y	v_z	p_g	B_t	ψ
1.0000E+0	0.0000E+0	0.0000E+0	0.0000E+0	1.0000E+0	1.0000E+0	0.0000E+0
7.1663E−1	5.7721E−1	−5.5635E−1	0.0000E+0	5.7331E−1	3.6182E−1	0.0000E+0
7.1663E−1	5.7721E−1	−1.3821E+0	1.5500E−1	5.7331E−1	3.6182E−1	2.7705E+0
8.8441E−1	3.4211E−1	−1.2343E+0	9.7515E−2	8.1650E−1	2.4919E−1	2.7705E+0
6.4152E−1	3.4211E−1	−1.2343E+0	9.7515E−2	8.1650E−1	2.4919E−1	2.7705E+0
3.2365E−1	−5.3327E−1	−7.7425E−1	−8.1532E−2	2.3419E−1	4.7503E−1	2.7705E+0
3.2365E−1	−5.3327E−1	−7.2576E−1	1.0345E−1	2.3419E−1	4.7503E−1	3.0000E+0
4.0000E−1	0.0000E+0	0.0000E+0	0.0000E+0	3.3333E−1	1.0000E+0	3.0000E+0

$B_n = 1.25$.

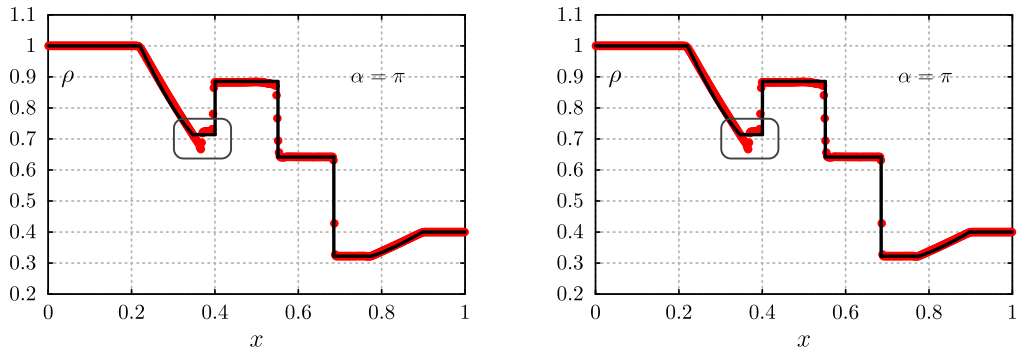

Fig. 5. Non-convergence for the coplanar case of Test 2. An irregular structure (fast compound wave) in the approximate solution exists in place of the rotational discontinuity in the exact solution at $x = 0.365$.

the downstream state through a rarefaction wave (i.e., a compound wave). Thus, conservative finite volume schemes cannot converge to the r-solution for cases involving a 180°, or near 180° rotation. This is especially problematic for low-resolution grids because a greater amount of numerical diffusion is expected [1,24].

Numerical diffusion also produces compound waves in Riemann problems with initial conditions near a critical state with a non-unique solution [24]. For these problems, the angle between the perpendicular magnetic fields separated by the initial discontinuity, called the twist angle α, determines uniqueness. Solutions for $\alpha \neq n\pi$, with $n \in \mathbb{Z}$ are unique. Compound waves appear in numerical solutions on coarse grids as α approaches $n\pi$ [24]. A compound wave connecting non-planar states, i.e. $\alpha \neq n\pi$, does not satisfy the Rankine–Hugoniot equations (2.6)–(2.10) and a numerical solution containing one is therefore not correct. As numerical diffusion is decreased through grid refinement, the compound wave loses its structure and the regular waves emerge. Torrilhon [24] called this property pseudo-convergence because convergence is initially towards the c-solution; divergence from the c-solution only occurs when enough diffusion is eliminated through grid refinement. The solution for various levels of grid refinement are shown for a near-coplanar case in Fig. 6. Torrilhon [24] reported that a simulation using 20 000 grid points had not completely converged to the r-solution. Pseudo-convergence also occurs in non-planar MHD Riemann problems with initial conditions near a critical state with a non-unique solution. The CWM technique for removing pseudo-convergence is described in the following section. Although a near-coplanar case is used for an example, CWM can be applied to non-planar problems as well.

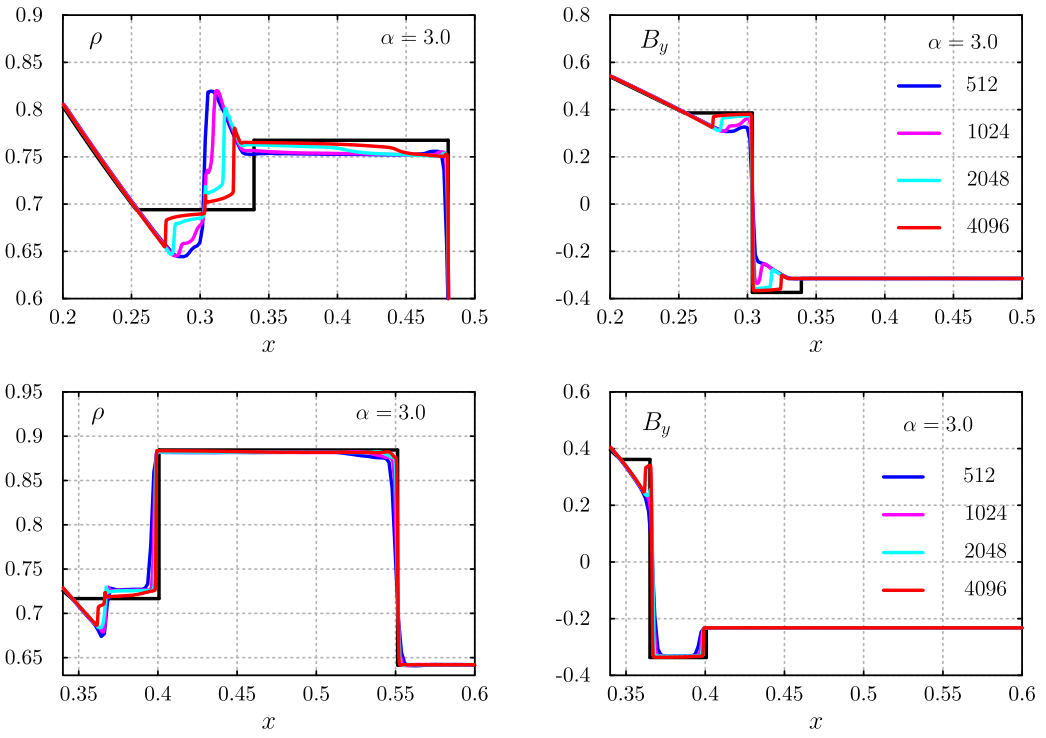

Fig. 6. Pseudo-convergence for a near-coplanar cases of Test 1 (top) and Test 2 (bottom). As the grid is refined from 1024 and 2048 points, the solution begins to diverge from the c-solution.

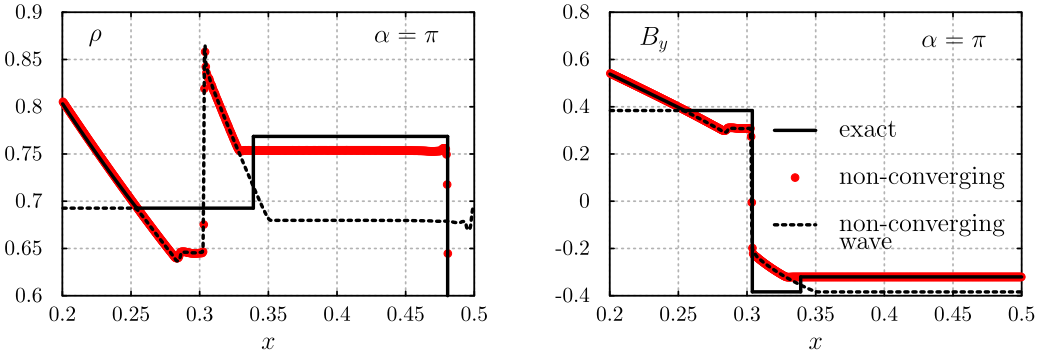

Fig. 7. The approximated slow compound wave (dashed black line), approximate non-converging c-solution (dotted red line), and exact r-solution (solid black line) for the coplanar case of Test 1. (For interpretation of the references to color in this figure legend, the reader is referred to the web version of this article.)

4. Convergence with finite volume schemes

4.1. Compound wave modification

The influence of a compound wave on the numerical solution can be minimized by limiting the artificial perturbation in pressure caused by numerical diffusion. We do this by subtracting flux so that only the perpendicular momentum and the magnetic field orientation are affected and thus the upstream and downstream states will still satisfy the jump conditions for a rotational discontinuity. The subtracted flux is chosen to be proportional to the flux contribution of the compound wave. We refer to this as compound wave modification (CWM) and its use in conjunction with HLLD as HLLD-CWM. The flux responsible for the formation of the compound wave is approximated by considering a reduced Riemann problem with initial conditions defined by the states upstream and downstream of the rotational discontinuity. The states correspond to $\mathbf{U}_l^*$ ($\mathbf{U}_{2r}^*$) and $\mathbf{U}_{2l}^*$ ($\mathbf{U}_r^*$) shown in Fig. 2 and Fig. 3 in the case of a left- (right)-going wave. The regular solution to the reduced Riemann problem consists of only one wave, a rotational discontinuity, separating two states. The flux between the two states produces a compound wave in numerical simulations as shown in Fig. 7.

The numerical solution to the coplanar Riemann problem as well as the solution to the reduced Riemann problem of Test 1 are shown in Fig. 7. The exact values for the initial conditions to the reduced Riemann problem are listed in the second and third rows of Table 1. In practice, the intermediate states are approximated since the exact solution is unknown. Three left-going structures are visible in the numerical solution to the reduced Riemann problem (dashed black line in Fig. 7). The intermediate shock at $x \approx 0.3$ is directly followed by a slow rarefaction whose head is located at $x \approx 0.3$ and tail at $x \approx 0.32$. The speed at the head of the slow rarefaction equals the speed of the intermediate wave, $v - c_a$, and the two structures move together forming a compound wave. The third structure in the compound wave solution is a fast rarefaction that connects the upstream state of the intermediate shock to the initial conditions. The speed at the head of the fast rarefaction (dashed black line in Fig. 7) is equal to the speed at the tail of the fast rarefaction in the solution to the full coplanar Riemann problem (solid black line in Fig. 7). These two fast rarefactions, one in the regular solution to the full Riemann problem and one in the compound wave, form a single structure in the compound wave solution to the full coplanar Riemann problem (dotted red line in Fig. 7). The compound wave solution also produces a right-going slow rarefaction wave that connects the state downstream of the left-going slow rarefaction wave to the initial right-state. The change in density through the right-going slow rarefaction is equal to the difference in density between the exact solution and compound wave solution downstream (left) of the contact discontinuity, at $x \approx 0.48$ in Fig. 7. The compound wave solution requires four structures, as opposed to one in the regular solution (i.e., the rotational discontinuity), to connect two intermediate states in full Riemann problem.

It is important to limit the removal of the flux responsible for producing the compound wave in a way that does not affect the solution in other parts of the domain. In CWM, the flux is modified if the cell is located in a discontinuity region with a near-180° rotation. Cell i is considered to be in such a region when $|\alpha_{i+1} - \alpha_{i-1}| > 2.5$ rad. This criteria ensures that the flux across regular shocks, waves, or contact discontinuities remains unchanged, but rotational discontinuities with a large change in α are affected. If this criteria is met, the intercell flux (2.18) becomes

$$\mathbf{F} = \mathbf{F}(\mathbf{U}_l, \mathbf{U}_r) - \begin{cases} A\mathbf{F}(\mathbf{U}_l^*, \mathbf{U}_{2l}^*) & \text{if } 0 \geq S_m, \\ A\mathbf{F}(\mathbf{U}_{2r}^*, \mathbf{U}_r^*) & \text{if } S_m < 0, \end{cases} \tag{4.1}$$

where $\mathbf{F}(\mathbf{U}_l, \mathbf{U}_r)$ is the flux associated with the full Riemann problem, $\mathbf{F}(\mathbf{U}_l^*, \mathbf{U}_{2l}^*)$ or $\mathbf{F}(\mathbf{U}_{2r}^*, \mathbf{U}_r^*)$ is the flux associated with the reduced Riemann problem depending on the direction of the middle wave, S_m (Eq. (39), [18]) is the velocity of the middle wave (i.e., contact discontinuity) shown in Fig. 3, and A is a user-specified constant. In this work, we set $A = 0.1$ in Test 1 and $A = 0.04$ in Test 2.

Approximating the intermediate states, $\mathbf{U}_\mathbf{j}^*$, does not require any additional computations because they are approximated during the initial HLLD flux evaluation. As described above, the intermediate states become the left and right state of the reduced Riemann problem if the change in orientation of the tangential magnetic field is greater than 2.5 radians. If a large rotation is not detected, the intercell flux, $\mathbf{F} = \mathbf{F}(\mathbf{U}_l, \mathbf{U}_r)$, is unmodified. The additional steps required for CWM are listed below.

1. Calculate the change in orientation of the tangential magnetic field between the left and right states. If it is larger than a user defined value, we use 2.5 radians, proceed to step 2.
2. Calculate $\mathbf{F}(\mathbf{U}_l^*, \mathbf{U}_{2l}^*)$ or $\mathbf{F}(\mathbf{U}_{2r}^*, \mathbf{U}_r^*)$ and modify the original flux according to (4.1).

The extra computations needed for CWM reduce the cell updates per CPU second by 1.25 times. We have also implemented it to run on devices capable of shared memory parallelism, e.g., multi-core CPUs and graphics processing units (GPUs). As expected, the performance ratio, a decrease of 1.25 times, was the same for multi-cores and serial runs on the CPU. The greater computational power of the GPU produced a smaller decrease of 1.15 times in performance. The decrease in performance with CWM is small considering an order of magnitude increase in grid resolution is required to achieve similar results with the unmodified HLLD scheme (see Section 4.2).

The intermediate states can also be calculated to machine precision with the nonlinear solver described in Section 2.3.1, however, doing so is computationally expensive. We implemented the nonlinear solver in version 4.2 of Athena to determine the computational costs. Compared to the HLLD approximate Riemann solver, we found an order of magnitude decrease in cell updates per CPU second when the nonlinear Riemann solver was used for flux evaluations.

The solution to the near-coplanar problems of Test 1 and Test 2 using Courant numbers of 0.8 and 0.1 is shown in Fig. 8 and Fig. 9 respectively. Noise downstream of the rotational discontinuity can be eliminated by lowering the Courant number. Alternatively, artificial viscosity in the form of [16,17] can be applied directly behind the rotational discontinuity to reduce the noise. The size of the region over which the artificial viscosity should be applied is problem specific. If too much is applied before the waves have separated, the slow wave behind the rotational discontinuity can become very diffuse. In schemes that apply a background diffusion, such as Flux Corrected Transport schemes [2], CWM does not produce any oscillations at higher Courant numbers.

In the unmodified solution for the near-coplanar case of Test 1, the state between the left-going slow shock, at $x = 0.331$, and the contact discontinuity, at $x = 0.481$, converges to the exact solution, but at different rates. The state should be constant throughout the region, but directly downstream of the left-going slow shock, the solution differs from the exact by $\approx 0.7\%$. The difference directly downstream of the contact discontinuity is $\approx 2\%$. For the coplanar case, the solution in

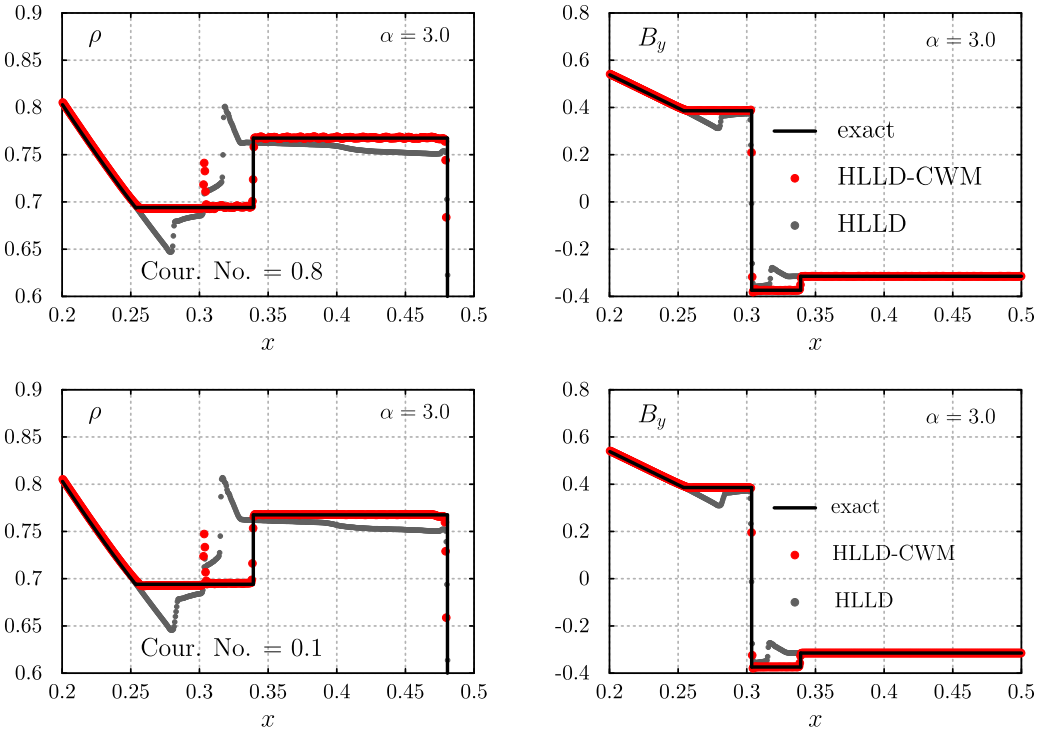

Fig. 8. The HLLD-CWM approximate solution and the exact r-solution to the near coplanar case of Test 1 on a grid of 2048 points. The compound wave is removed except near $x = 0.303$.

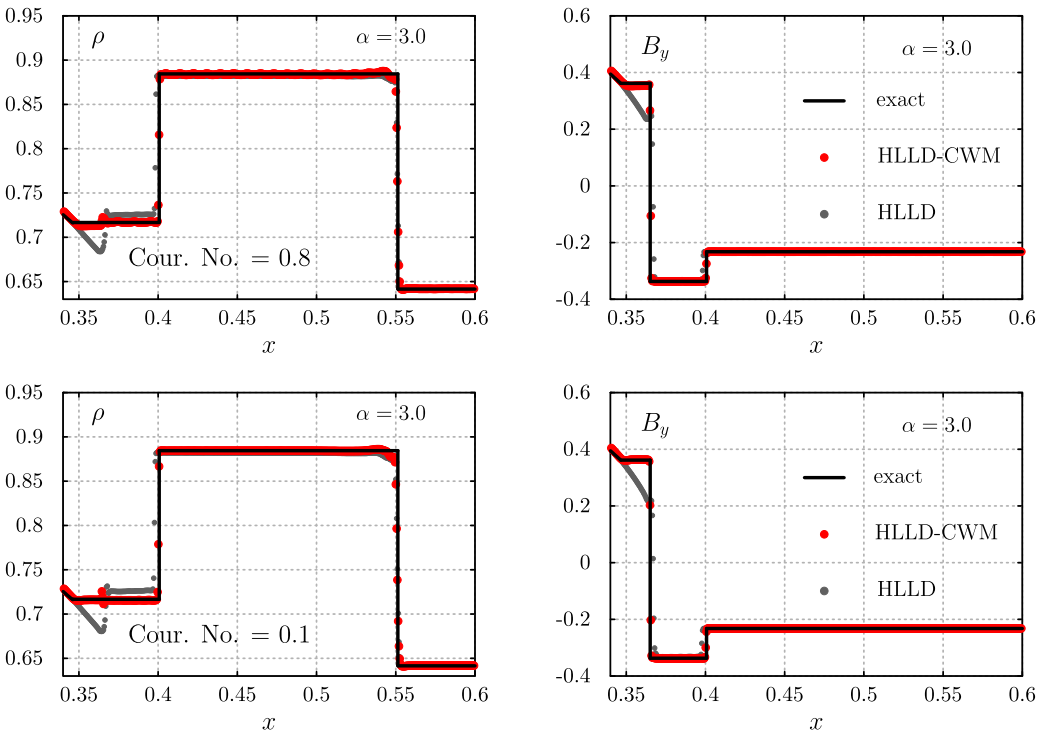

Fig. 9. The HLLD-CWM, HLLD approximate solutions, and the exact r-solution to the near coplanar case of Test 2 on a grid of 2048 points. The compound wave is removed except near $x = 0.365$.

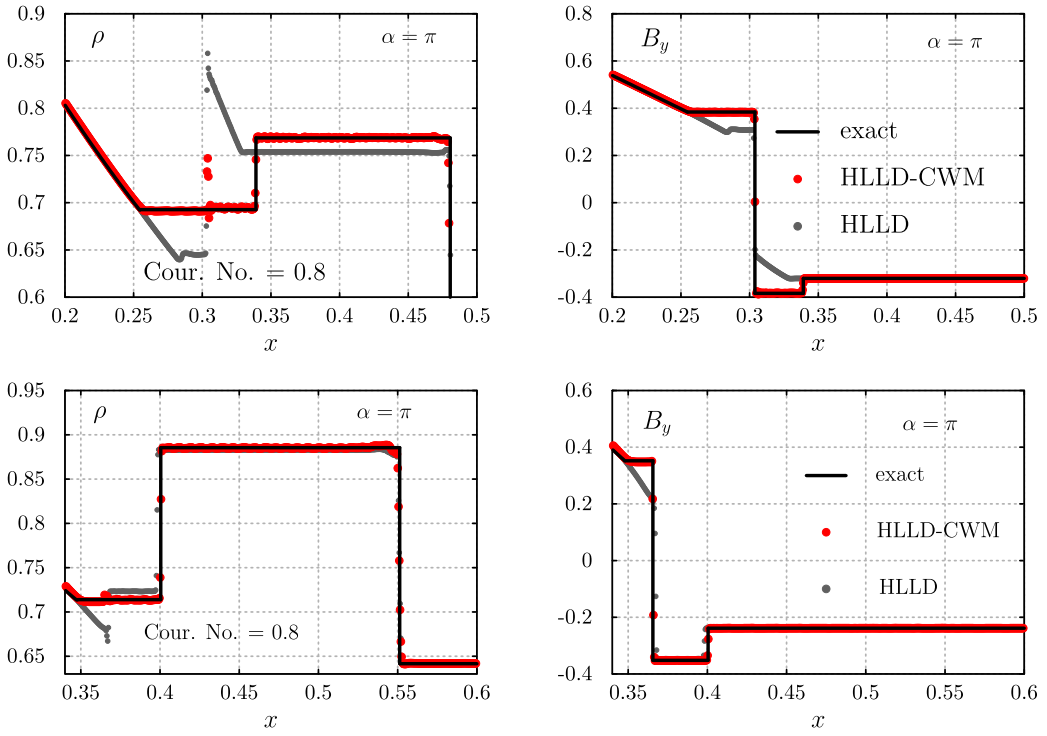

Fig. 10. The HLLD-CWM, HLLD approximate solutions, and the exact r-solution to the coplanar cases of Test 1 (top) and Test 2 (bottom) on a grid of 2048 points. The compound wave of Test 1 is removed except near $x = 0.303$, and the compound wave of Test 2 is removed except near $x = 0.365$.

this region remains constant, but differs from the exact solution by $\approx 3\%$. These issues are eliminated with HLLD-CWM. The appearance of the rotational discontinuity and slow shock is independent of the value of α and the regular structures are present and have correct values for the state variables in both cases.

As shown in Fig. 8 (top row of Fig. 10) and less so in Fig. 9 (bottom row of Fig. 10) for the near coplanar cases (coplanar cases), the transition across the rotational discontinuity is unresolved. The CWM procedure removes the compound wave from the solution except in this layer and leaves a deviation from the exact solution as the rotational discontinuity is crossed. In order to remove the deviation, the transition region where the tangential magnetic field changes sign must be detected, unless an exact solver is used, in which case the location is known. A point is considered to be within the transition region of a 180° rotation if $|\alpha_{i+2} - \alpha_{i-2}| > 2.5$ rad. The states at these points must be adjusted in order to satisfy the jump conditions of a rotational discontinuity: $[\rho] = [v_n] = [p_g] = [B_\perp^2] = 0$, $\pm\sqrt{\rho}[v_y] = [B_y]$, $\pm\sqrt{\rho}[v_y] = [B_y]$ $\pm\sqrt{\rho}[v_z] = [B_z]$, and $[E] = \pm\sqrt{\rho}[\mathbf{v}\cdot\mathbf{B}]$. A straight-forward adjustment is to have points with a rotation angle less (greater) than $\pi/2$ be assigned the value of the upstream (downstream) value outside of the transition. Although this approach produces acceptable results for the considered one-dimensional cases, it is not conservative because mass, momentum, and energy are removed.

4.2. Error analysis

In this section we present the results of RMSE calculations for the coplanar and near coplanar cases of Test 1. Only the domain $x = [0.254, 0.481]$ where the HLLD and HLLD-CWM solutions differ is considered in error calculations. This is the region between the tail of the left-going fast rarefaction and the right-going contact discontinuity (CD). The region includes either a left-going slow shock and rotational discontinuity or a compound wave (see Fig. 8).

The RMSE was computed using

$$\text{RMSE} = \sqrt{\sum_{i=1}^{M} \mathcal{E}_i^2},$$

and

$$\mathcal{E} = \frac{1}{N}\sum_{i=1}^{N} \left| U_i - U_{ex}(x_i) \right|$$

where M is the number of conservative state variables, N is the number of gridpoints, U_i is an approximated conservative state variable, and U_{ex} is the exact solution for the conservative state variable.

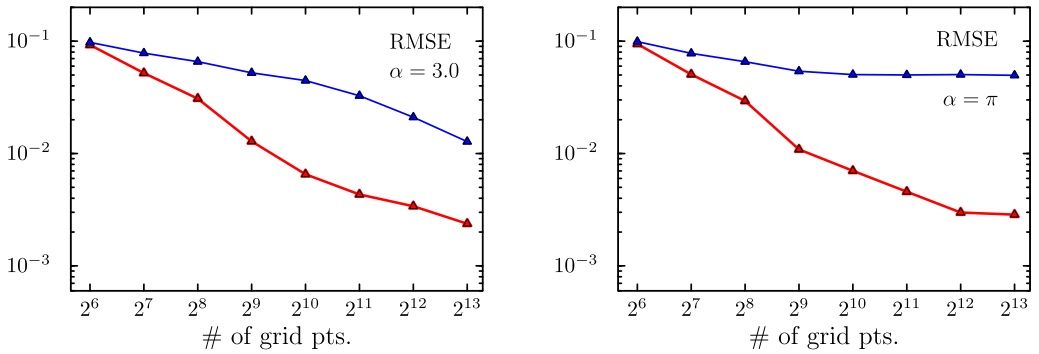

Fig. 11. RMSE in $x = [0.254, 0.481]$ using HLLD (blue) and HLLD-CWM (red). (For interpretation of the references to color in this figure legend, the reader is referred to the web version of this article.)

The RMSEs of the original HLLD scheme and the modified HLLD-CWM scheme for both the coplanar and near-coplanar cases of Test 1 are shown in Fig. 11. For the near-coplanar case, a reduction in RMSE through grid refinement occurs with both HLLD and HLLD-CWM. Initially convergence is much quicker with HLLD-CWM. As numerical diffusion is decreased through grid refinement, the compound wave breaks apart and the convergence rate using HLLD increases at about 2^{10} grid points. For the coplanar case, the RMSE is reduced through grid refinement only when the HLLD-CWM flux is used. Note that the domain used in this analysis differs slightly from $x = [0.2, 0.4]$ used in [24]; the domain used here covers the largest differences between the exact and non-converging solution.

5. Conclusion

A modification to the finite volume method can be used to produce the correct solutions to non-unique Riemann problems of ideal MHD equations. The properties of the planar ideal MHD equations discussed in [10] were used to describe the appearance of compound wave structures in finite volume approximations. The flux is modified near a large rotation ($\alpha > 2.5$) so that the upstream and downstream states satisfy the jump conditions for a rotational discontinuity. The method may be well suited for simulations in two- and three-dimensions because it does not track the rotational discontinuity.

The CWM method also gives true convergence for problems with initial conditions near those with a non-unique solution. It is the first flux approximation for a dissipative finite volume scheme that does not exhibit pseudo-convergence. The number of grid points required to obtain RMSEs on the order of 10^{-2} is reduced by an order of magnitude for the near coplanar case.

The CWM method can be applied in simulations on a wide range of spatial scales, but it is best suited for large-scale simulations for two reasons: smoothing oscillations caused by over-shoots downstream of the Alfvén wave is required for small scale simulations and the greatest reduction in L^1-errors are achieved at lower resolutions.

The CWM method should be tested with other methods of approximating numerical fluxes in FVMs. For Roe-type methods that use solutions to the linearized system of equations, the intermediate states can be approximated as linear combinations of the eigenvalues and eigenvectors of the Jacobian (Eq. (3.19), [19]). The HLLD method is convenient to use with the CWM method because it gives the exact solution to an isolated rotational discontinuity [18] and its intermediate states provide an initial guess that results in a high rate of convergence when a nonlinear solver is used. If a nonlinear solver is used, more frequent calls may be required for problems in two- and three- dimensions. In this case, reducing the number of iterations can decrease computational costs without a loss in accuracy of the final solution. It is important to stress that the results presented here using CWM were obtained exclusively with the HLLD approximate Riemann solver. Although a nonlinear solver may potentially improve the accuracy of CWM, it is not required. That is a unique property of CWM.

References

[1] A.A. Barmin, A.G. Kulikovskiy, N.V. Pogorelov, J. Comput. Phys. 126 (1996) 77–90.
[2] J.P. Boris, D.L. Book, J. Comput. Phys. 11 (1973) 38–69.
[3] M. Brio, C.C. Wu, J. Comput. Phys. 75 (1988) 400–422.
[4] J.K. Chao, L.H. Lyu, B.H. Wu, A.J. Lazarus, T.S. Chang, R.P. Lepping, J. Geophys. Res. 98 (1993) 17443–17450.
[5] P. Colella, P.R. Woodward, J. Comput. Phys. 54 (1984) 174–201.
[6] W. Dai, P.R. Woodward, J. Comput. Phys. 111 (1994) 354–372.
[7] H. de Sterck, B.C. Low, S. Poedts, Phys. Plasmas 5 (1998) 4015–4027.
[8] H. de Sterck, S. Poedts, Phys. Rev. Lett. 84 (2000) 5524–5527.
[9] B. Einfeldt, P.L. Roe, C.D. Munz, B. Sjogreen, J. Comput. Phys. 92 (1991) 273–295.
[10] S.A.E.G. Falle, S.S. Komissarov, J. Plasma Phys. 92 (2001) 29–56.
[11] H. Feng, J.M. Wang, Sol. Phys. 247 (2008) 195–201.
[12] T. Inoue, S. Inutsuka, Prog. Theor. Phys. 118 (2007) 47–58.

[13] A. Jeffrey, Magnetohydrodynamics, Oliver & Boyd, London, 1966.
[14] A. Jeffrey, T. Taniuti, Non-linear Wave Propagation, Academy Press, New York, 1964.
[15] L.D. Landau, E.M. Lifshitz, L.P. Pitaevskii, Electrodynamics of Continuous Media, 2nd edition, Course in Theoretical Physics, vol. 8, Pergamon Press, Oxford, 1984.
[16] A. Lapidus, J. Comput. Phys. 2 (1967) 154–177.
[17] R. Löhner, K. Morgan, O.C. Zienkiewicz, Comput. Methods Appl. Mech. Eng. 51 (1985) 441–465.
[18] T. Miyoshi, K. Kusano, J. Comput. Phys. 208 (2005) 315–344.
[19] D. Ryu, T.W. Jones, Astrophys. J. 442 (1995) 228–258.
[20] J. Stone, T. Gardner, P. Teuben, Athena MHD code project, https://trac.princeton.edu/Athena/, 2010.
[21] J.M. Stone, T.A. Gardiner, P. Teuben, J.F. Hawley, J.B. Simon, Astrophys. J. Suppl. Ser. 178 (2008) 137–177.
[22] K. Takahashi, S. Yamada, J. Plasma Phys. 79 (2013) 335–356.
[23] M. Torrilhon, Research report 2002-06, Seminar for applied mathematics, ETH Zurich, 2002.
[24] M. Torrilhon, J. Comput. Phys. 192 (2003) 73–94.
[25] M. Torrilhon, J. Plasma Phys. 69 (2003) 253–276.
[26] M. Torrilhon, D.S. Balsara, J. Comput. Phys. 201 (2004) 586–600.
[27] C.C. Wu, Geophys. Res. Lett. 14 (1987) 668–671.
[28] C.C. Wu, J. Geophys. Res. 93 (1988) 3969–3982.
[29] C.C. Wu, J. Geophys. Res. 93 (1988) 987–990.
[30] C.C. Wu, J. Geophys. Res. 95 (1990) 8149–8175.
[31] C.C. Wu, C.F. Kennel, Geophys. Res. Lett. 19 (1992) 2087–2090.